

# Evaluation of lensing in photonic crystal slabs exhibiting negative refraction

Zhi-Yuan Li and Lan-Lan Lin

*Ames Laboratory and Department of Physics and Astronomy, Iowa State University, Ames, Iowa 50011, USA*

(Received 2 September 2003; published 12 December 2003)

We systematically investigate lensing of electromagnetic waves by a negative refractive-index material slab constructed from a two-dimensional photonic crystal with properly designed equifrequency-surface configuration [Luo *et al.*, Phys. Rev. B **65**, 201104 (2002)]. We find that a point source placed in the vicinity of the slab can form a good-quality image in the opposite side of the slab. However, the image is strongly confined in the near-field region of the slab and gradually degrades and disappears when moved beyond the near-field domain. In addition, the image-slab distance has little dependence on the source-slab distance and the slab thickness. On the other hand, the image can also form by a slab with a positive effective refractive index. We have analyzed the equifrequency-surface contour configuration of this photonic crystal and found that the overall imaging properties of this photonic crystal slab are dominantly governed by the self-collimation effect and complex near-field wave scattering effect, rather than by the all-angle negative-refraction effect.

DOI: 10.1103/PhysRevB.68.245110

PACS number(s): 78.20.Ci, 41.20.Jb, 42.70.Qs

## I. INTRODUCTION

Recently there appears renewed interest in and some controversies over materials that can exhibit a negative refraction behavior,<sup>1–13</sup> called left-handed materials or negative refractive-index materials (NIM's). When an electromagnetic (EM) wave beam is incident from air on a NIM slab, the refraction beam follows Snell's law for a negative refractive index, and propagates into the material on the negative side of the surface normal, inverse to our everyday experiences. One famous example towards a NIM is a metamaterial built from arrays of copper split-ring resonators and copper wire strips.<sup>3–6</sup>

It was shown that negative refraction could also occur in lossless dielectric photonic crystal structures.<sup>12,13</sup> The equifrequency surface of Bloch's modes can be properly designed so that the group velocity (directed to the equifrequency-surface normal) of a Bloch's mode excited by an incident wave is pointed to a negative-refraction direction. In particular, Luo *et al.* showed that all-angle negative refraction could be achieved at the lowest band of two-dimensional (2D) photonic crystals and at a wavelength four times larger than the lattice constant, which allows for easier achievement of homogeneous refraction of wave beams. An important application of a NIM is superlensing. Pendry predicted that a NIM slab could behave as a "perfect" lens with a resolution well below the diffraction limit based on the argument that a NIM slab can enhance and retrieve the evanescent wave components involved in the radiation from a point source.<sup>7</sup> Numerical analysis by Luo *et al.* seemed to justify this superlensing envision through the all-angle negative-refraction mechanism. Yet, the photonic structure still witnesses a strong wave scattering effect at the concerned frequency domain as it is made up of high dielectric cylinders (with a dielectric constant  $\epsilon$  around 14) with modest filling fractions (around 0.3) and a modest scalar effective refractive index (around 2). In this strong scattering regime, there might be various factors that can contribute to the observed imaging phenomenon associated with the inhomogeneous medium. Then it is an interesting and important task to

extract the dominant mechanism among all these possible factors that contributes most to the observed phenomenon. A good routine to evaluate a superlens is to see whether it works by simple refraction law (although negative) or something else like the complicated near-field effect. This is concerned because all NIM's to date are artificial inhomogeneous media, yet they are approximated as effective homogeneous media. In this paper we will try to evaluate this problem by looking more closely into the 2D photonic crystal NIM investigated by Luo *et al.*

## II. DEPENDENCE OF IMAGING EFFECT ON SLAB THICKNESS AND OBJECT DISTANCE

To see whether the lens made from a NIM slab is dominantly governed by the negative-refraction mechanism, we have taken a simple starting point that is easy to conceive and understand from the well-known conventional lensing laws. Suppose that lensing by a NIM slab is indeed described by negative beam refraction, then the lensing mechanism can be depicted by the simple pictures in Fig. 1 similar to those presented in Refs. 2 and 7. In Fig. 1(a) a point source *A* is placed at a distance  $d_1$  from the left surface of a NIM slab of thickness  $w$ . The radiation wave first refracts through the slab by a negative angle and converges back to a point. After released from the slab the wave reaches a focus for a second time, and becomes the image *B* under observation (at a dis-

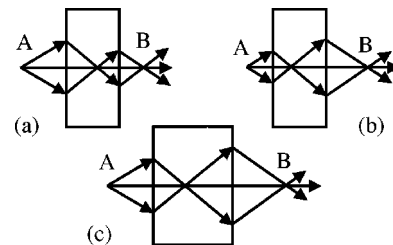


FIG. 1. Schematic pictures depicting the lensing of a source *A* by a NIM slab to an image *B*. (a), (b), and (c) represent imaging in different source distances and slab thicknesses.

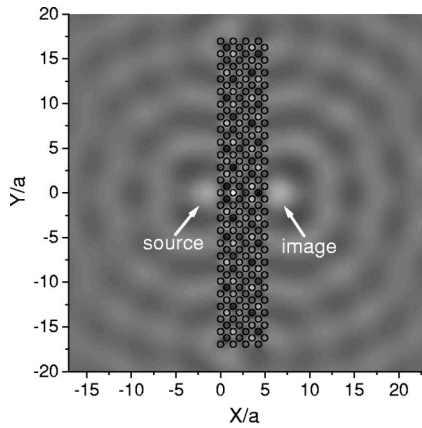


FIG. 2.  $E_z$  field patterns of a point source placed at  $x = -0.5a$  and its image across an eight-layer 2D photonic crystal slab at frequency  $\omega = 0.192(2\pi c/a)$ . Dark and bright regions correspond to negative and positive  $E_z$ , respectively.

tance  $d_2$  from the right surface of the slab). From simple ray-trace analysis as shown in Figs. 1(b) and 1(c), one can find that when the source is closer to the slab, or the slab becomes thicker, the image distance will be increased. The image shift with respect to the change in  $d_1$  and  $w$  strongly depends on the refractive index of the NIM. But one thing can be certain, if the physical mechanism behind the lensing is indeed a wave-beam refraction through an effective homogeneous NIM, one should observe the aforementioned image shift.

The system we examine is a 2D photonic crystal slab consisting of a square lattice of dielectric cylinders in air and with the surface normal along the  $\Gamma M$  [(11)] direction. The cylinder has a dielectric constant of  $\epsilon = 14$  and a radius of  $r = 0.3a$ , where  $a$  is the lattice constant. This structure has been studied in Ref. 13, according to which the slab exhibits an all-angle negative refraction behavior and consequently a superlensing effect at a narrow frequency window centered around  $\omega = 0.192(2\pi c/a)$  for the TM polarization mode. We have reexamined this system and employed a highly efficient and accurate multiple-scattering approach<sup>14,15</sup> to calculate propagation of EM wave emitting from a monochromatic TM-polarized point source at  $\omega = 0.192(2\pi c/a)$ . A typical result of the  $E_z$  field pattern is shown in Fig. 2 for a slab  $25\sqrt{2}a$  wide and eight layers thick. The geometry of the photonic crystal slab is also displayed. In all structures considered in this paper, the center of the cylinders in the first layer is always set to locate at  $x = 0$ , and the slab is symmetric with respect to  $y = 0$ . In Fig. 2, the point source is placed at  $x = -0.5a$  and  $y = 0$ , very close to the surface of the slab (located at  $x = -r$ ), corresponding to a source distance of  $d_1 = 0.2a$ . One can find quite a high quality image formed in the opposite side of the slab. The significant point is that the field patterns in the two hand sides of the slab exhibit good identity, and look as if diverging from two point sources. A closer look at the data reveals a transverse size (full size at half maximum) of the image spot as  $2.5a$ , or  $0.48\lambda$ . The image is centered at  $x = 6.8a$  and  $y = 0$ , corresponding to an image distance of  $d_2 = 1.6a$ . Our result is in agreement with

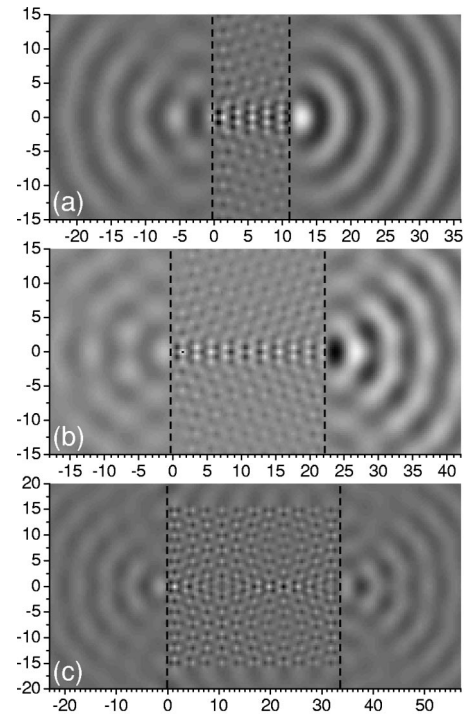


FIG. 3.  $E_z$  field patterns of a point source placed at  $x = -0.5a$  and its image across a 16-, 32-, and 48-layer photonic crystal slab in (a), (b), and (c), respectively. The slab surfaces are represented by two dashed lines.

Ref. 13, and seems to verify that the photonic crystal slab can act as a superlens. However, more evidences are required before definite conclusion can be drawn on the dominant physical mechanism hiding behind the observed phenomenon.

To this end, we have changed the source distance  $d_1$  and the slab thickness  $w$ , and see what happens to the imaging by the slab. The calculated field patterns for a source fixed at  $x = -0.5a$  and  $y = 0$  before a photonic crystal slab with 16, 32, and 48 layers of cylinders are displayed in Figs. 3(a), 3(b), and 3(c), respectively. For the 16-layer slab, a well-shaped bright image spot is formed. This image spot is peaked at  $x = 12.8a$ , still very close to the right surface of the slab (located at  $x = 10.9a$ ). The corresponding image distance is  $d_2 = 1.9a$ , only a slight forward shift from the image formed by the eight-layer slab. The image spot is elongated in the lateral direction, while contracted in the longitudinal direction. Having a closer look at the field pattern inside the slab, one can clearly find a rectangular bright pattern connecting the source and the image spots, which has a lateral size close to the source and image spot sizes. No apparent focusing of wave is found inside the slab. Instead, it seems that the wave transmitting into the slab is first collimated, then travels across the slab via this confined wave front, much like a wave transmitting through a photonic crystal waveguide. The radiation pattern from this waveguide exit will appear as if the wave is diverging from an image spot. The physical mechanism leading to this self-collimation effect will be discussed and become clear in Sec. IV.

A similar guiding effect can also be found in thicker slabs.

In Fig. 3(b), the 32-layer slab has two surfaces located at  $x = -0.3a$  and  $x = 22.2a$ . The emitting wave travels through the central narrow guiding channel (with a lateral size of about  $2.5a$ ), and forms a dark image spot in the vicinity of the right surface. The peak locates at  $x = 23.8a$  and  $y = 0$ , corresponding to an image distance  $d_2 = 1.6a$ . The field pattern shows some aberrations, indicating that the imaging of this slab is somewhat degraded compared to the eight-layer slab. The distortion of image is further amplified for the 48-layer slab, however, the imaging effect is still visible. The dominant image spot is a dark one and is peaked at  $x = 36.8a$  and  $y = 0$ , with  $d_2 = 3.3a$ . A slightly weaker bright spot is closer to the right surface, and locates at  $x = 24.8a$  and  $y = 0$ , corresponding to  $d_2 = 1.3a$ . In addition, the central guiding channel in this slab is not as regular as those in the 16- and 32-layer slabs, whose shape and lateral size strongly vary when the wave transverses the slab.

From Figs. 2 and 3, one can find that imaging effect does exist in the considered photonic crystal slab. However, one can also find that the image distance does not have a simple dependence on the slab thickness expected for a NIM lens which works dominantly under the well-known wave-beam refraction law as depicted in Fig. 1(c). Actually, the image spot is always located in the vicinity of the surface of the lens, in another words, in the near-field domain. To have a more complete vision on the imaging effect of this type of NIM material, we have changed the source distance  $d_1$ , and see what happens to the imaging behavior of the lens. Figures 4(a)–4(d) display the calculated  $E_z$  field patterns for a source placed at  $x = -a$  and  $y = 0$  (corresponding to  $d_1 = 0.7a$ ) before four different photonic crystal slabs consisting of 8, 16, 32, and 48 layers of cylinders. The calculated field patterns for  $d_1 = 1.7a$  are displayed in Figs. 5(a)–5(d) for the four slabs. In all cases, a visible image is formed. However, all images are located in the near-field domain of the slab, and a guiding channel is clearly visible connecting the near-field source and image spots for thicker slabs. In addition, the dependence of the image position does not follow the simple picture depicted in Fig. 1(b) expected for a NIM lens which works dominantly under Snell's law for wave-beam refraction. These observations at least indicate that the negative-refraction effect is not the dominant factor governing the near-field imaging behavior.

### III. IMAGING BEYOND THE NEAR-FIELD SPACE DOMAIN AND THE NEGATIVE-REFRACTION FREQUENCY DOMAIN

In the above we have seen that a source placed at the near-field region of the NIM slab always forms an image also at the near-field region of the opposite side of the slab, dominantly through the formation of a guiding channel within the NIM slab. In our next step we move the light source well beyond the near-field space domain. We have found that the imaging effect of these slabs strongly degrades and finally disappears. Such a situation can be well represented by two typical examples depicted in Figs. 6 and 7, where the calculated field pattern formed by a point source placed at a position of  $x = -4a$ ,  $-8a$ , and  $-20a$ , respectively, before a

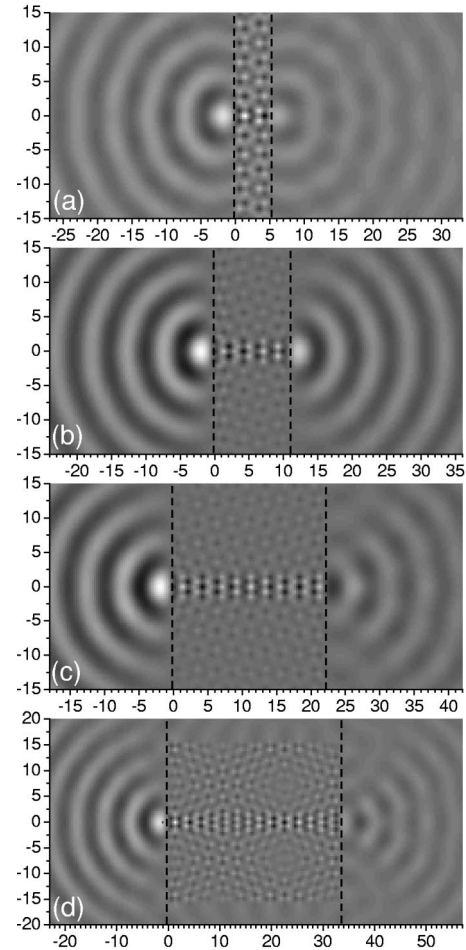


FIG. 4.  $E_z$  field patterns of a point source placed at  $x = -a$  and its image across an 8-, 16-, 32-, and 48-layer photonic crystal slab in (a), (b), (c), and (d), respectively.

16-layer and a 32-layer photonic crystal slab are displayed. As the light source radiates at a frequency of  $0.192(2\pi c/a)$ , or a wavelength of  $5.2a$ , the light source in all the three situations is obviously located beyond the near-field space domain of the slab. All these field patterns have a common characteristic. When the diverging EM waves emitted from the point source impinge on the photonic crystal slab, they are collimated by the slab and travel across the slab along a highly regular high-intensity guiding channel. In the opposite side, EM waves once again diverge in the form of highly regular oscillating radiation patterns, but now they do not look as if radiating from a pointlike source as in Figs. 2–5, but rather from a slitlike source. The width of the guiding channel and the radiation slit grows when the source-slab distance increases. This also means that the imaging functionality of the slab gradually degrades.

We have seen that the formation of a near-field image by the photonic crystal slab depends largely on the guiding channel formed within the slab and very little on the negative refraction expected for this NIM. Keeping this in mind, we might expect that a slab with a positive effective refractive index (satisfying everyday experiences of light refraction) can also serve as a near-field lens. We have tried to lower the excitation frequency of the monochromatic source and go

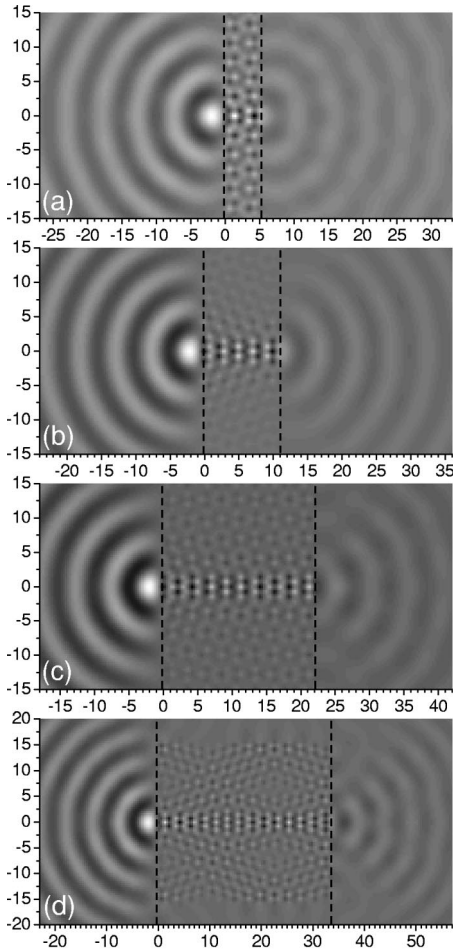


FIG. 5.  $E_z$  field patterns of a point source placed at  $x = -2a$  and its image across an 8-, 16-, 32-, and 48-layer photonic crystal slab in (a), (b), (c), and (d), respectively.

sufficiently beyond the all-angle negative-refraction frequency window of the photonic crystal, and indeed found imaging effect existing at some geometric parameters. Figures 8(a) and 8(b) show two such examples. In Fig. 6(a), the source is at frequency  $\omega = 0.17(2\pi c/a)$ , and placed at  $x = -a$  and  $y = 0$  before a eight-layer slab. In Fig. 6(b), the source is at frequency  $\omega = 0.15(2\pi c/a)$ , and placed at  $x = -a$  and  $y = 0$  before a 16-layer slab. In both structures, an image spot is clearly visible, which can be justified from the regular out-going oscillation-decaying field patterns expected for a point source. The image spot is still located in the near-field domain of the surface, and a guiding channel is also visible connecting the source and the image, but the guiding channel is far less regular than at  $\omega = 0.192(2\pi c/a)$ , at which negative refraction is expected. Since the two frequencies are both located in the positive-index domain of the crystal, we see that negative refraction is not an indispensable factor in the formation of a near-field image by the inhomogeneous slab.

We have continued to lower the excitation frequency of the light source, and find that in some situations, a near-field image, although greatly degraded, still can form. An example is shown in Fig. 8(c), where the source is at frequency  $\omega$

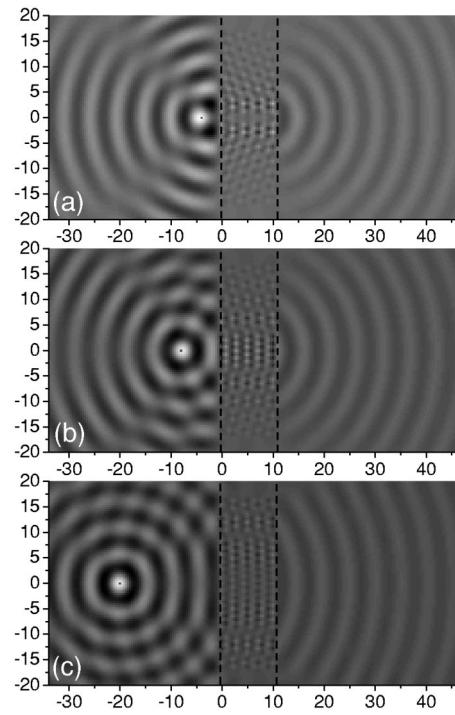


FIG. 6.  $E_z$  field patterns of a point source and its image across a 16-layer photonic crystal slab at frequency  $\omega = 0.192(2\pi c/a)$ . The light source is placed beyond the near-field space domain and locates at  $x = -4a$ ,  $x = -8a$ , and  $x = -20a$  in (a), (b), and (c), respectively.

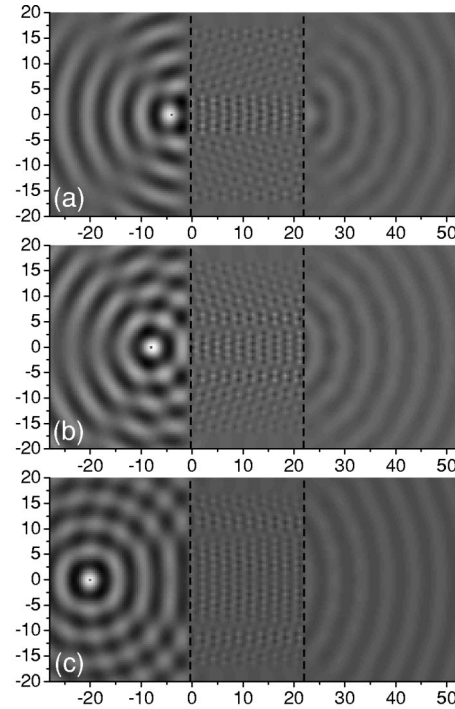


FIG. 7.  $E_z$  field patterns of a point source and its image across a 32-layer photonic crystal slab at frequency  $\omega = 0.192(2\pi c/a)$ . The light source is placed beyond the near-field space domain and locates at  $x = -4a$ ,  $x = -8a$ , and  $x = -20a$  in (a), (b), and (c), respectively.

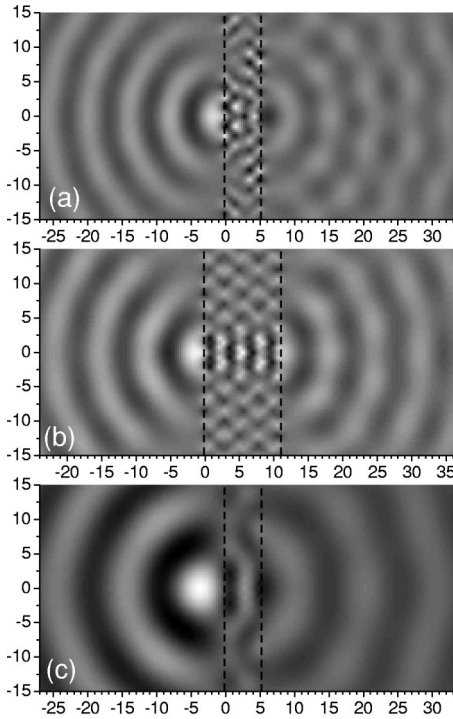


FIG. 8.  $E_z$  field patterns of a point source and its image for (a) an eight-layer slab at frequency  $\omega=0.17(2\pi c/a)$ ; (b) a 16-layer slab at frequency  $\omega=0.15(2\pi c/a)$ ; and (c) an eight-layer slab at frequency  $\omega=0.1(2\pi c/a)$ . The point source is placed at  $x=-a$  in (a) and (b), and  $x=-4a$  in (c).

$=0.1(2\pi c/a)$  (or a wavelength of  $10a$ ), and placed at  $x=-4a$  and  $y=0$  before an eight-layer slab. Even at this long-wavelength domain, there still exist regular out-going radiation patterns in the opposite side of the slab, which can be said to diverge from a black spot in the vicinity of the right surface of the slab. Since the wavelength is about two times the slab thickness, no apparent guiding channel can be found within the slab. This phenomenon might be better explained by a complex scattering effect occurring in the near-field domain, where the EM wave will not witness the optical properties of the bulk photonic crystal material as an effective homogeneous medium.

We have also considered imaging by thick photonic crystal slabs. We find that no guiding channel is formed within the slab, and as a result no apparent imaging effect exists for these samples. Figure 9 displays the calculated field patterns for a near-field point source placed at  $x=-a$  and  $y=0$  before a 48-layer thick slab. The source is excited at frequency 0.17, 0.15, and  $0.1(2\pi c/a)$  in Figs. 9(a), 9(b), and 9(c), respectively. It is clear that the thick slabs can not serve as a near-field lens at a frequency domain beyond the all-angle negative-refraction frequency window. The remarkably different imaging properties of a thin slab and a thick slab, as can be found by comparing Fig. 8 with Fig. 9, indicate that the imaging effect for a thin slab may be induced dominantly by a complex wave-scattering effect in the near-field space domain and in the long-wavelength regime.

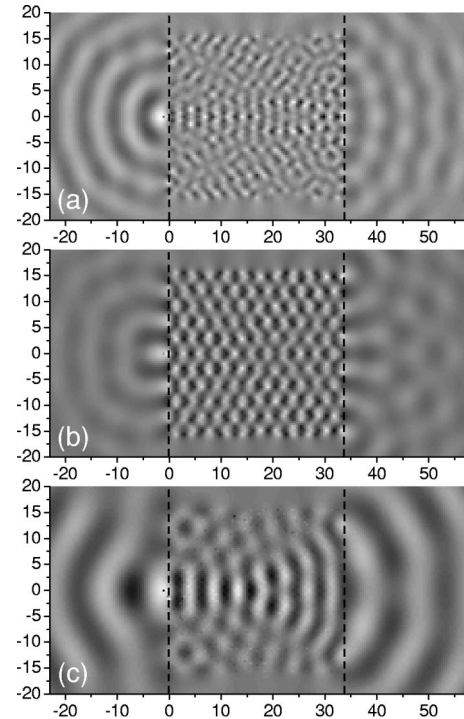


FIG. 9.  $E_z$  field patterns of a point source and its image for a 48-layer thick slab at frequency (a)  $\omega=0.17(2\pi c/a)$ ; (b)  $\omega=0.15(2\pi c/a)$ ; and (c)  $\omega=0.1(2\pi c/a)$ . The point source is all placed at  $x=-a$ .

#### IV. IMAGING VIEWED FROM EQUIFREQUENCY-SURFACE CONFIGURATIONS

The propagation of EM waves through a photonic crystal, which is a highly inhomogeneous medium in its nature, usually witnesses some strong scattering effects. This makes it difficult to describe the propagation behavior in a simple yet accurate way. However, recently a lot of theoretical and experimental practices<sup>12,13,16-18</sup> have shown that the overall behavior of the wave propagation within a photonic crystal can be well described, at least qualitatively, by a model based on the equifrequency-surface configuration of the photonic crystal and the related group velocity, which is parallel to the equifrequency-surface normal direction.

We have employed a plane-wave expansion method<sup>19,20</sup> to calculate the TM-mode band structures and equifrequency-surface contours of the photonic crystal discussed in the above sections. The results are displayed in Figs. 10(a) and 10(b), respectively. 441 plane waves are adopted in the calculation, and good convergence has been reached. 1681 Bloch's wave vectors within the first Brillouin zone are used in constructing the equifrequency surface contour. As can be seen in Fig. 10(a), a complete TM band gap opens between the first and second bands, and lies at frequencies  $0.214-0.283(2\pi c/a)$ . The dashed line represents the frequency  $0.192(2\pi c/a)$ , at which negative refraction occurs. It is located in the fundamental band, but is close to the band edge. Therefore some strong scattering effect can be expected.

In Fig. 10(b), the equifrequency-surface contours at several relevant frequencies such as 0.1, 0.15, 0.17, and

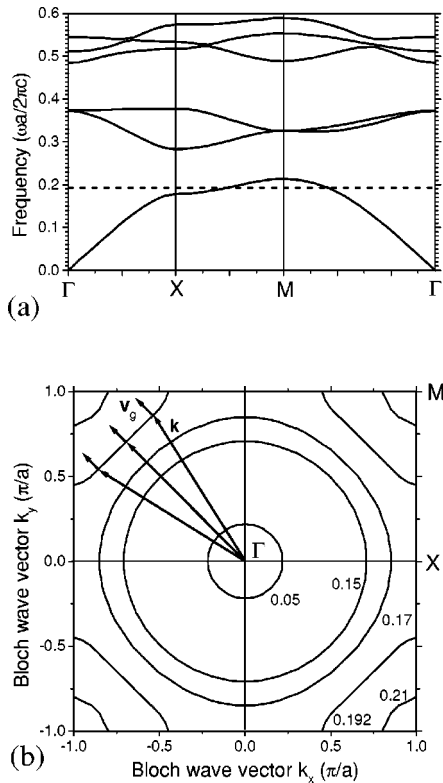


FIG. 10. (a) Photonic band structures and (b) equifrequency-surface contour plots for the 2D photonic crystal studied in this paper. The photonic crystal is composed of a square lattice of dielectric cylinders with  $\epsilon=14$  and  $r=0.3a$  embedded in the air background, and is excited at the TM polarization mode.

0.192( $2\pi c/a$ ) are demonstrated. All curves are convex everywhere. The 0.1 and 0.15 contours are very close to a perfect circle, and therefore the group velocity at any point of the contour is collimated with the  $\mathbf{k}$  vector, indicating that the crystal behaves like an effective homogeneous medium at these two long wavelengths. The 0.17 contour is a little bit distorted from a circle, with the distance  $|\mathbf{k}|$  along the (11) direction slightly (about 3%) shorter than along the (10) direction. The 0.192 contour is significantly distorted from a circle. In most part of the contour (part-I domain), which is centered around the (11) direction, the curve is quite flat and has the surface normal pointing to the (11) direction, while in the other small part (part-II domain) near the Brillouin-zone edge (line XM), the surface normal is directed towards the M point. As the group velocity  $\mathbf{v}_g(\mathbf{k})$  for a given Bloch's mode characterized by  $\mathbf{k}$  is parallel to the equifrequency-surface normal at this  $\mathbf{k}$  point, we see that the group velocities of the excited Bloch's wave within the photonic crystal in the part-II domain is pointed towards the M point, and corresponds to an apparent negative refraction direction for the photonic crystal slab studied above, which has a surface normal parallel to (11) direction. In contrast, in the part-I domain, the group velocity would point dominantly along the (11) direction, and at most slightly leans (within a few degrees) towards the negative refraction direction. Perhaps this is why the term of all-angle negative refraction is entitled to this photonic crystal slab in Ref. 13. At the (11) direction, the

group velocity is exactly collimated with the wave vector.

The equifrequency-surface contour configuration in Fig. 10(b) can help us to qualitatively explain some of the imaging properties of the photonic crystal slab. First of all, a collimation over external incident diverging waves can be expected for the slab, especially for those wave components confined within a modest incident angle consistent with the part-I domain in Fig. 10(b). Such a self-collimation feature has been found in other NIM and photonic crystal structures.<sup>16–18</sup> This feature can well explain a highly regular guiding channel found in Figs. 6 and 7, where the source is well away from the slab and has a relatively small diverging angle with respect to the slab. It can also contribute to the formation of a less regular guiding channel in Figs. 3–5, where the light source is located within the near-field domain of the slab. Yet, in these latter structures, the self-collimation feature can be intertwined with the complex near-field scattering effect as well as the negative refraction for the wide angle wave components in determining the complex propagation behavior of the wave through a thick slab, such as those found in Figs. 3(c), 4(d), and 5(d). In the near-field domain, the slab does not behave dominantly as an effective homogeneous medium whose refraction properties are governed by the equifrequency-surface contour configuration. As the excitation frequency is lowered to 0.17, 0.15, and 0.1 ( $2\pi c/a$ ), the self-collimation effect is absent according to the nearly circular equifrequency-surface contours shown in Fig. 9(b). In these situations, the formation of a near-field image in Figs. 8(a)–(c) may be induced by complex near-field scattering effect for these relatively thin slabs.

The above numerical simulations and analyses over the equifrequency-surface contour configuration all indicate that the imaging effect in the photonic crystal structures is not governed by the simple refraction law expected for a NIM, but rather by a self-collimation effect intertwined with complex near-field wave-scattering effect. As a comparison, the all-angle negative-refraction effect contributes little to the imaging behavior of this photonic crystal NIM. In addition, no apparent retrieval of the evanescent wave information exist in the current structure, as can be most clearly seen in Figs. 6 and 7. This is in contrast to the analysis made in Ref. 7 for a NIM. In Ref. 13, another photonic crystal made from air cylinders in a dielectric background and excited by the TE polarization mode is shown to exhibit an all-angle negative-refraction effect in a certain low-frequency window, at which the near-field imaging effect also happens. As the equifrequency-surface contour configuration there (see Fig. 1 in Ref. 13) is very similar to Fig. 10(b) here, it is more likely that the imaging effect observed in Ref. 13 is also dominantly induced by the self-collimation and near-field scattering effects rather than the all-angle negative-refraction mechanism.

## V. SUMMARY

In summary, we have systematically investigated lensing of EM waves by a certain 2D photonic crystal NIM slabs. We find that point sources placed in the vicinity of the slab can form images by the slab. However, the image is strongly

confined in the near-field region, and the image distance has little dependence on the source distance and the slab thickness. A guiding channel has been found to form within the slab connecting the near-field source and image. When the source is moved beyond the near-field space domain, the imaging effect strongly degrades. On the other hand, near-field image can also form by a slab with a positive effective refractive index. We have analyzed the equifrequency-surface contour configuration of this photonic crystal and found that the formation of the guiding channel is induced by the collimation feature of the group velocity associated with the excited Bloch's wave within the photonic crystal. The overall imaging properties of this photonic crystal slab are dominantly governed by the self-collimation effect and complex near-field wave scattering effect. As a comparison, the all-angle negative-refraction mechanism cannot explain satisfactorily the observed imaging behaviors. These indicate

that the imaging by this particular material is not a simple refraction behavior expected from Snell's law for an effective homogeneous NIM, and thus not "lensing" in its traditional meaning. We hope that the analysis presented for this particular NIM material will stimulate assessment of the superlensing effect in other NIM materials.<sup>3-7</sup> An efficient route towards evaluation of the real physical mechanism behind an observed complex imaging phenomenon may be the investigation of the role which the refraction law might play in the formation of the image.

#### ACKNOWLEDGMENT

Ames Laboratory is operated for the U.S. Department of Energy (DOE) by Iowa State University under Contract No. W-7405-Eng-82.

- 
- <sup>1</sup>J.B. Pendry, *Opt. Express* **11**, 369 (2003).  
<sup>2</sup>V.G. Veselago, *Usp. Fiz. Nauk* **92**, 517 (1964) [*Sov. Phys. Usp.* **10**, 509 (1968)].  
<sup>3</sup>J.B. Pendry, A.J. Holden, D.J. Robbins, and W.J. Stewart, *J. Phys.: Condens. Matter* **10**, 4785 (1996).  
<sup>4</sup>D.R. Smith, Willie J. Padilla, D.C. Vier, S.C. Nemat-Nasser, and S. Schultz, *Phys. Rev. Lett.* **84**, 4184 (2000).  
<sup>5</sup>R.A. Shelby, D.R. Smith, and S. Schultz, *Science* **292**, 77 (2001).  
<sup>6</sup>A.A. Houck, J.B. Brock, and I.L. Chuang, *Phys. Rev. Lett.* **90**, 137401 (2003).  
<sup>7</sup>J.B. Pendry, *Phys. Rev. Lett.* **85**, 3966 (2000).  
<sup>8</sup>N. Garcia and M. Nieto-Vesperinas, *Phys. Rev. Lett.* **88**, 207403 (2002).  
<sup>9</sup>P.M. Valanju, R.M. Walser, and A.P. Valanju, *Phys. Rev. Lett.* **88**, 187401 (2002).  
<sup>10</sup>J. Pacheco, Jr., T.M. Grzegorzczak, B.I. Wu, Y. Zhang, and J.A. Kong, *Phys. Rev. Lett.* **89**, 257401 (2002).  
<sup>11</sup>S. Foteinopoulou, E.N. Economu, and C.M. Soukoulis, *Phys. Rev. Lett.* **90**, 107402 (2003).  
<sup>12</sup>M. Notomi, *Phys. Rev. B* **62**, 10 696 (2000).  
<sup>13</sup>C. Luo, S.G. Johnson, J.D. Joannopoulos, and J.B. Pendry, *Phys. Rev. B* **65**, 201104 (2002).  
<sup>14</sup>L.M. Li and Z.Q. Zhang, *Phys. Rev. B* **58**, 9587 (1998).  
<sup>15</sup>Z.Y. Li and K.M. Ho, *Phys. Rev. B* **68**, 045201 (2003).  
<sup>16</sup>H. Kosaka, T. Kawashima, A. Tomita, M. Notomi, T. Tamamura, T. Sato, and S. Kawakami, *Appl. Phys. Lett.* **74**, 1212 (1999).  
<sup>17</sup>R.W. Ziolkowski and E. Heyman, *Phys. Rev. E* **64**, 056625 (2001).  
<sup>18</sup>D.N. Chigrin, S. Enoch, C.M. Sotomayor Torres, and G. Tayeb, *Opt. Express* **11**, 1203 (2003).  
<sup>19</sup>K.M. Ho, C.T. Chan, and C.M. Soukoulis, *Phys. Rev. Lett.* **65**, 3152 (1990).  
<sup>20</sup>Z.Y. Li, J. Wang, and B.Y. Gu, *Phys. Rev. B* **58**, 3721 (1998).